CHAPTER 5

MODULATION OF SYNOPTIC-SCALE CONVECTION

"A challenging task for atmospheric scientists is to try to delineate the physical nature of the individual disturbances and their dynamical relationship. Without substantial progress toward this goal, forecasting the weather and climate in the monsoon region would remain a routine exercise of empiricism."

— Mankin Mak, 1987

5.1 Synoptic-Scale Variability

While the ISO is the dominant mode of intraseasonal variability in the South Asian monsoon, a second type of higher frequency intraseasonal variability is also present (see Fig. 1.2). This mode is composed of high-frequency, 5–10-day, wavelike phenomenon, including westward propagating synoptic-scale vorticity waves (Lau and Lau 1990) as well as monsoon depressions and lows (for extensive review of these synoptic-scale systems, see Meehl 1987). These storms typically form in the Bay of Bengal or in the western Pacific Ocean and propagate westward and north-westward into the Ganges River valley (Krishnamurti *et al.* 1977; Saha *et al.* 1981). Large precipitation amounts accompany these disturbances and

can lead to flooding, especially in the lowlands of northeast India and Bangladesh. Together with the ISO, these two modes of variability explain up to 60% of the intraseasonal variance of the South Asian monsoon (see Section 5.2 for details).

The prominence of the two modes of variability is readily seen in raw precipitation timeseries. Figure 5.1a is a histogram of the average daily accumulated precipitation in the western Bay of Bengal for June and July, 1992. Two active periods of rainfall are separated by about 30–40 days, the first extending from June 12 to June 22 and the second somewhat less well-defined extending from around July 15 through July 27. A break period separates the two active periods and is marked by about 2–3 weeks of reduced, although not negligible, rainfall. Comparing the precipitation timeseries of Fig. 5.1a with the latitude-time precipitation section along 85°–90°E in Fig. 5.1b, one observes that the active periods at latitudes 15°–20°N appear to be the product of a northward propagation of precipitation that begins in the central equatorial Indian Ocean and propagates to 20°–25°N at this longitude. Figures 5.1c and 5.1d are time-longitude sections of precipitation along 15°–20°N and 0°–5°N, respectively. Along both latitude swathes, two slowly moving eastward progressions of precipitation are seen within the June to July period with the equatorial precipitation leading the northern precipitation. Higher frequency oscillations in rainfall are also clearly visible in Fig. 5.1. For example, in Fig. 5.1a, there are numerous instances when local peaks in precipitation are separated by 5–10-days, e.g., June 15 to June 20 and July 11 to July 16 to July 24. Examination of these dates on the time-longitude diagram (Fig. 5.1c) reveals that the aforementioned peaks in precipitation often can be linked to westward propagating systems. In the first time period, June 14 to June 19, the systems are relatively short lived, originating in the eastern portion of the Bay of Bengal and quickly moving across

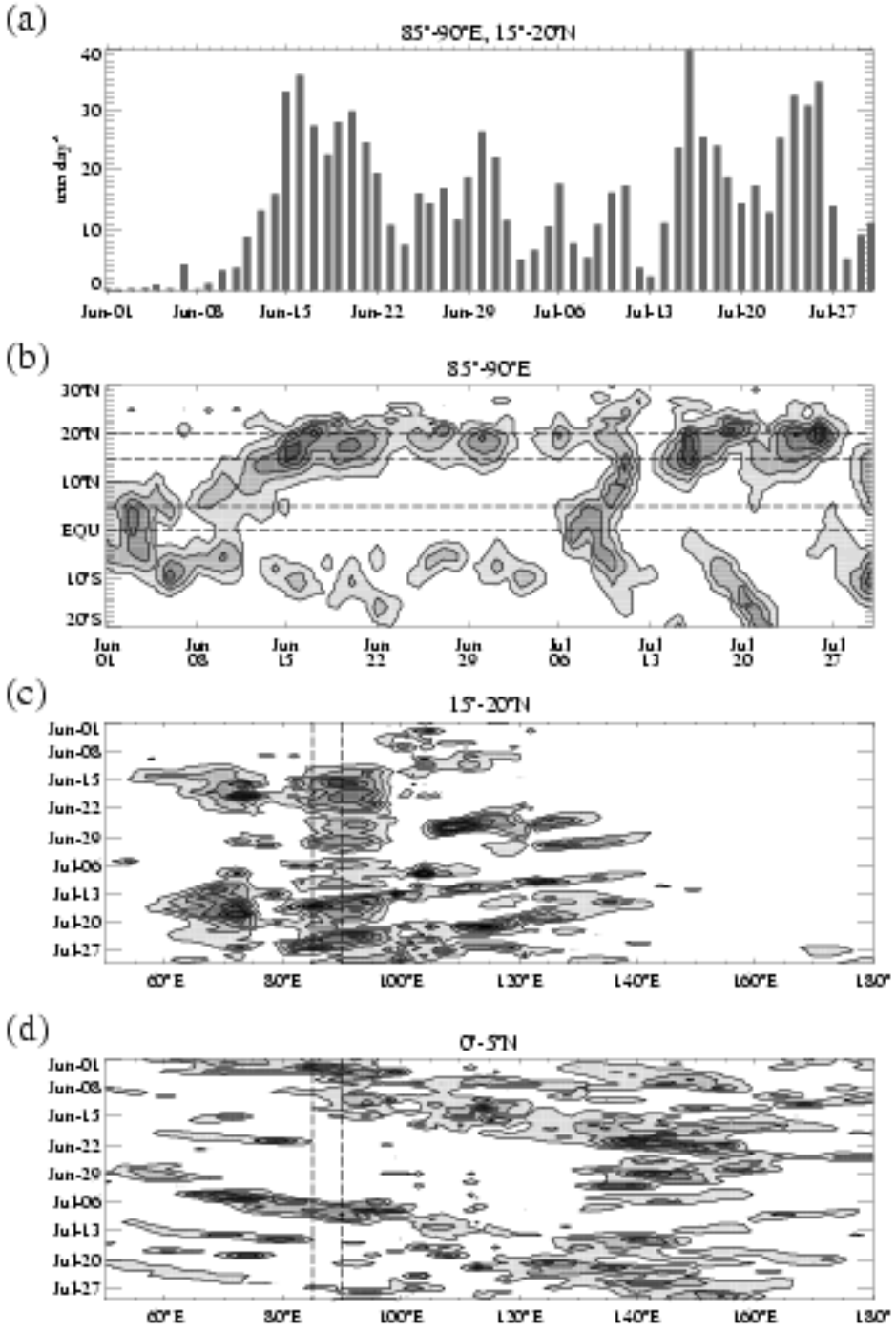

Figure 5.1. Daily precipitation rate estimates for June and July of 1992 monsoon season. (a) Precipitation in Bay of Bengal averaged over 85°-90°E, 15°–20°N. Time-latitude and time-longitude sections of precipitation along (b) 85°–90°E, (c) 15°–20°N, and (d) 0°–5°N. Contour intervals are 7.5 mm day^{-1}.

to the east coast of India at which point they continue northwestward up the Ganges river basin. It is also relevant to note that these westward propagating waves occur during the convective or active phase of the ISO. During the latter period, July 11 through July 24, the waves originate as far east as 140°E. The relatively heavy precipitation around June 30 that divides up the break epoch may also be attributable to a westward propagating system originating over the western Pacific Ocean warm pool. During this time period, a low-level cyclone moves westward across the western Pacific Ocean, weakens as it crosses the southeast Asian peninsula, and re-intensifies upon reaching the warm waters of the Bay of Bengal; a sequence that is reminiscent of that described by Krishnamurti *et al.* (1977). Westward propagating waves, such as these, are described and cataloged by Lau and Lau (1990; Lau and Lau (1992) although they make no distinction between those that are restricted to the Bay of Bengal and those whose origin is in the western Pacific Ocean.

Clearly, the northern summer monsoon intraseasonal variability is complex. The above discussion of Fig. 5.1 raises questions about how the two predominant modes of intraseasonal variability, the large-scale ISO and the westward propagating synoptic-scale waves, interact with and impact each other. Does the northward propagation of the ISO excite westward propagating disturbances or is the apparent northward propagation of the ISO a time-averaged manifestation of the high-frequency waves? Also, are the westward propagating systems that strike India during a break period excited by the ISO when it reaches the western Pacific Ocean, or are they a result of the inherent instability of the easterly vertical wind shear that is a characteristic of the Asian monsoon?

In a modeling study, Lau and Peng (1990) found that the interaction between the large-scale monsoon flow and the equatorial intraseasonal oscillation results in the generation of unstable westward propagating baroclinic disturbances with spatial scales of approximately 3000–4000 km and periods of 5–6 days. These spatial and temporal scales correspond reasonably to those scales identified by Lau and Lau (1990). The rapid growth of the disturbances over the Bay of Bengal and peninsular India is attributed to instability that is favored in regions of large easterly vertical wind shear (see Fig. 5.7b) and reduced effective static stability induced by the heating associated with the equatorial ISO. Xie and Wang (1996) found that, in general, a moist baroclinic instability is remarkably enhanced by easterly vertical shears. According to Lau and Peng, the enhanced convection in the monsoon region and the coincident rising motion draws low-level air northward, consequently weakening the equatorial convection and resulting in a rapid northward propagation of low-frequency convection. Murakami (1984), Krishnamurti *et al.* (1985), and Wang and Rui (1990) have all observed an increase in high-frequency westward propagating wave activity associated with the northward propagating arm of the ISO. Furthermore, it has been shown that tropical cyclones, storms and depressions are more often excited during the convective phase of the ISO rather than during the suppressed phase (Liebmann *et al.* 1994).

The aforementioned studies support the observation Fig. 5.1 that high-frequency waves are excited during active periods over India. However, the theories put forth do not address the source of westward propagating convective systems that occur during large-scale break phases of the monsoon. Wang and Xie (1997) hypothesize that westward propagating waves emanate from the western Pacific Ocean when the Kelvin-Rossby wave packet disintegrates after it stalls near the dateline

where the SST decreases, subsequently reducing moist static energy and thus convection over the eastern equatorial Pacific. It is also possible that the anomalous easterly zonal vertical wind shear associated with the ISO (Madden and Julian 1971; Knutson *et al*. 1986) acts to destabilize the atmosphere in the western Pacific region, exciting unstable waves such as those described by Xie and Wang (1996).

This chapter is structured as follows. Section 5.2 is devoted to a wavenumber-frequency analysis of OLR in the Asian monsoon region, similar to that done in Section 3.2.2 but now including higher frequency variability. A cross-correlation and linear regression analysis is used in Section 5.3 to identify the time evolution of the circulations associated with the two dominant timescales. Wavelet analysis is used to develop a measure of the intensity of high-frequency wave activity in Section 5.4. Subsequently, a composite analysis is employed to investigate the relationship between the ISO and westward propagating wave activity. Section 5.5 describes a canonical intraseasonal variability sequence that is developed in the previous sections.

5.2 Wavenumber-Frequency Spectra

5.2.1 Method Wavenumber-frequency spectral analysis is introduced in Section 3.2.2. Here, an ensemble mean wavenumber-frequency variance spectrum is calculated from individual wavenumber-frequency variance spectra generated from 22 122-day segments (June–September) for the years 1975–1997 and including each of the 5 gridded latitudes between 10°N and 20°N. The longitudinal domain includes the entire eastern hemisphere (0°–180°E). For each 122-day segment, the mean, the first three harmonics of the annual cycle and the linear trend are removed prior to space-time spectra calculations. In addition, each segment is tapered to zero with a 10% cosine taper in both time and space to reduce spectral

leakage and aliasing. The spatial dimension is padded with zeros in the segments outside the eastern hemisphere. This padding ensures that the resulting wavenumbers represent planetary scale wavenumbers. A detracting consequence of completing space-time spectra on a limited longitudinal domain is that the wavenumber resolution is reduced resulting in a spread of variance through adjacent wavenumbers. For example, for a 180° longitudinal domain, planetary wavenumbers 1, 3, 5, etc. are not properly resolved. So, variance that should be fully attributable to wavenumbers 1, 3, 5 etc. is spread into adjacent wavenumbers.

5.2.2 OLR Wavenumber-Frequency Variance Spectra The logarithm of the fractional OLR ensemble wavenumber-frequency variance spectrum is shown in Fig. 5.2a. A number of spectral peaks are discernible in the raw spectrum with the strongest peak seen at wavenumbers 1, 2, and 3 at a period of between 25 and 60 days, consistent with the timescale of the ISO. Although this peak is skewed towards the eastward manifold, significant, albeit weaker, variance is also seen in the westward manifold, especially at wavenumber 4.

Two other features of the raw OLR variance spectra are easily recognizable. The first is the prominent prejudice of variance to the westward manifold at higher frequencies. The second is the "redness" in both wavenumber and frequency, that is the variance increases with both decreasing wavenumber and decreasing frequency. This redness presents a challenge if one wishes to identify individual spectral peaks that are statistically significant. A final point to note about the raw spectrum is the obvious peaks at about eastward wavenumber 14 and periods of 9 and 4.5 days. These peaks, as noted by Wheeler and Kiladis (1999), are due to aliasing associated with the slow eastward precession of consecutive polar orbiting satellite

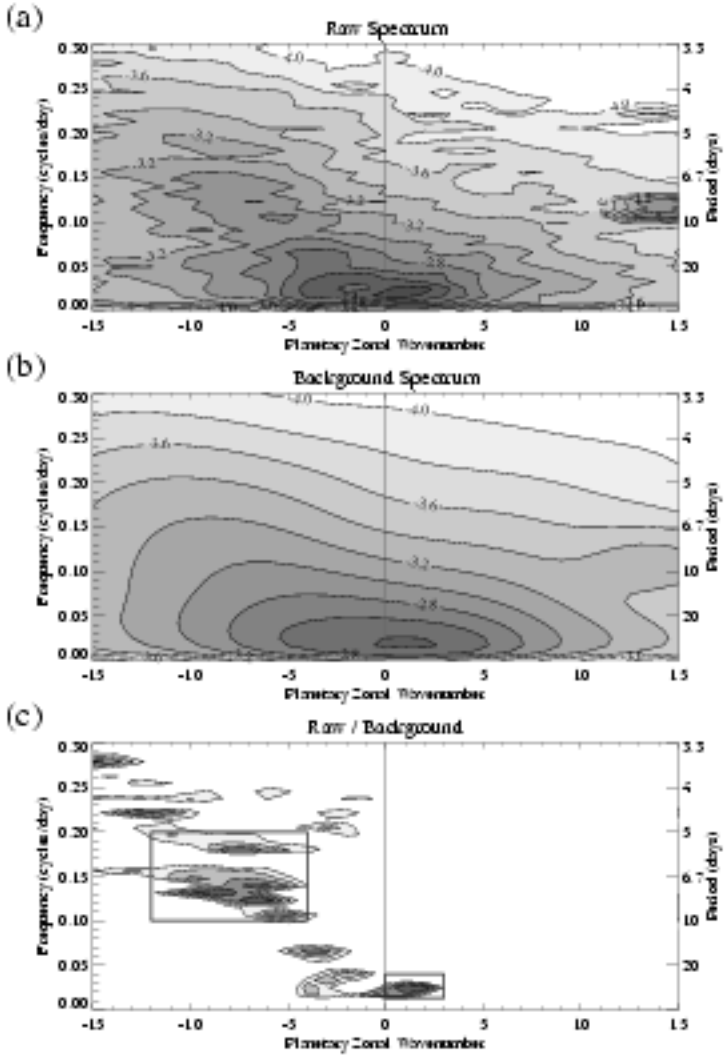

Figure 5.2. Zonal wavenumber-frequency variance spectra of anomalous OLR in longitudinal domain 0°–180°E. Variance spectra are composite spectra of 22 122-day segments (JJAS) representing the years 1975–1997 (excluding 1978). Power spectra for each year are calculated individually and then averaged for the five gridded latitudes between 10°–20°N. (a) Base-10 logarithm of fractional variance of raw composite variance spectrum. (b) Base-10 logarithm of fractional variance of background variance spectrum. Background variance is calculated by averaging individual variance spectra of 122-day segments over the entire record 1979-1997, and smoothing with a 1-2-1 filter in both wavenumber and frequency (see text for details). (c) Raw OLR variance divided by background variance. Shaded regions indicate wavenumber-frequency peaks that exceed the background variance at the 95% confidence level (based on 44 d.o.f.). Contour interval is 0.1 and shading begins at 1.0.

passes, a precession that takes 9 days to move one pass-width which is about 26° or wavenumber 14.

Clearly, in order to distinguish spectral peaks that rise substantially above the red spectrum, a red background spectrum is required. Here, the red background spectrum was generated, as in Wheeler and Kiladis (1999), by finding an ensemble mean variance spectrum, as described above for the raw OLR wavenumber-frequency variance spectrum, except now including the entire OLR data record from January 1975 to December 1997. The OLR time series is broken up into 122-day segments with each segment overlapping the previous segment by two months to make a total of 112 individual 122-day segments for each latitude. The raw background spectrum is then smoothed repeatedly with a 1-2-1 filter in both frequency (10 times at low-frequency to 40 times at high-frequency) and wavenumber (10 times). This smoothing largely eliminates the individual features of the raw spectrum. Use of the full record permits one to compare the JJAS spectrum relative to the average spectrum for the entire year. The resulting smoothed background variance spectrum (Fig. 5.2b) is red in both wavenumber and frequency. While this method of defining a background spectrum reduces the skew towards westward manifold variance, the skew is not eliminated entirely, indicating that the skew towards westward manifold variance is a feature that is endemic to the region. The distribution of variance between the two manifolds, however, is far more evenly distributed than when a background spectrum is generated from just the boreal summer months (not shown).

The raw OLR wavenumber-frequency variance spectrum divided by the smoothed background variance spectrum is shown in Fig. 5.2c. The two most prominent oscillations (a near 40-day oscillation and a 5–7-day oscillation) that were

found in the thotough spectral analysis of histotical Indian station tainfall data by Hartmann and Michelsen (1989), ate appatent in Fig. 5.2c. The ISO peak stands out at eastwatd wavenumbets 1–3 and petiods of 25–80-days. At this petiod, thete is also a weakly significant westwatd manifold peak at wavenumbet 4. A second ptominent featute is the conglometate of spectral peaks found at westwatd manifold wavenumbets 4–10 and petiods of 5–10-days. The individual peaks in this wavenumbet-frequency domain ate insepatable, but ate of similat timescale and wavelength as the "relative vottticity waves" identified in ptevious studies (e.g., Lau and Lau 1990; Lau and Lau 1992), and othet tropical disturbances such as monsoon depressions and tropical cyclones.

A final ptominent peak is seen at 15–20-day petiods at westwatd wavenumbets 2–6. A numbet of authots have found spectral peaks in the Asian monsoon tegion at this timescale (e.g., (Murakami 1977), 15 days; (Keshavamurty 1973), 10–20 days). In contiast, Hartmann and Michelsen (1989) found little evidence that such a ftequency is important for Indian tainfall with only a few stations in the far notth of India exhibiting spectial peaks within the 15–20-day timescale. Further analysis teveals that the 15–20-day peak disappeats when a mote limited longitudinal domain of 40°–100°E is used, implying that the oscillation is ptimatily encountered in the western Pacific Ocean tegion. The 15–20-day peak seen in Fig. 5.2c may be telated to the westwatd ptopagating 20–30-day mode identified by Mutakami (1980), Mutakami (1984), and Wang and Rui (1990) that is confined to the western Pacific and is not genetally obsetved in the ptimaty tegion of intetest.

This ptocedute was tepeated with the independent ptecipitation data, yielding qualitatively similat tesults (not shown) and thus confitming the tobustness of the ptominent spectral peaks. Wavenumbet-ftequency spectra calculated ftom the

entire globe provide greater wavenumber resolution, but the resulting spectrum (not shown) is more difficult to interpret due to strong western hemisphere OLR variance at 3–5-day periods at westward wavenumbers 10–15.

5.2.3 Wavenumber-Frequency Filtering Based on the results from the wavenumber-frequency spectral analysis, the OLR data is filtered into two wavenumber-frequency bands that are denoted by the black boxes in Fig. 5.2c. These bands are 5–10-days, westward wavenumbers 4 through 10 to capture the easterly tropical disturbances; and 25–80-days, eastward wavenumbers 1 through 3 to retain the ISO signal. These wavenumber-frequency bands represent 14% and 11% of the total intraseasonal OLR variance for the 40°–160°E, 10°–20°N area. A Fourier spectral analysis (not shown) in the Indian monsoon core region (70°–90°E, 10°–20°N) shows that the 5–10-day band contains 28% while the 25–80-day band represents 27% of the intraseasonal OLR variance. For details on the wavenumber-frequency filtering procedure see Wheeler and Kiladis (1999). Hereafter, the two wavenumber-frequency filtered bands will be identified as OLR_{5-10w} and OLR_{25-80e}, respectively where the "5-10" and the "25-80" reflects the periods retained and the "w" and the "e" reflect the westward and eastward wavenumbers retained.

5.3 Intraseasonal Oscillation and Synoptic-Scale Disturbances

5.3.1 Intraseasonal Oscillation The cross-correlation and linear regression method, described in Section 2.2.2, is first employed on the low-frequency 25–80-day timescale to illustrate the evolution of a typical summertime ISO. A 5° longitude by 5° latitude area in the central equatorial Indian Ocean (85°–90°E, 12.5°–17.5°N) is selected as the base region. The area-averaged OLR_{25-80e} in the base region is used as the predictive timeseries and is regressed against 25–80-day

filtered OLR and 25–80-day filtered u_{850} and v_{850}. The location of the base region is found to be unimportant with qualitatively similar results found using base regions located throughout the domain. A central Bay of Bengal base region was chosen primarily for clarity of presentation. Figure 5.3 shows the lagged regressions of OLR and the 850-mb wind every 5 days from lag –20 days to lag +20 days.

The typical evolution of the summer ISO, as described in Chapter 3, begins with the development of a central equatorial Indian Ocean convection anomaly (lag –20 days in this regression). Simultaneously, a large-scale suppressed convection anomaly is located over India. The break period is marked by anomalous northwesterly low level flow (flow that is opposite to the normal southwesterly monsoon flow) indicating a temporarily weakened monsoon. By lag –10 days, the break period over India is over and convection begins to appear over the southern Arabian Sea while the equatorial convection extends out over the maritime continent. A mature active period over India sets in by lag –5 days with equatorial convection now located over the warm pool in the western Pacific Ocean. The low level monsoon flow spins up over the next 10 days, reaching its maximum strength at lag +5 days; meanwhile, a suppressed convection anomaly appears along the equator. By lag + 10 days, the equatorial convection anomaly has gradually disappeared near the dateline, and all that remains is convection north of the equator along the southeast Asian coast. The 850-mb anomalous westerly winds have pushed eastwards into the western Pacific Ocean. At lag +20 days, with the suppressed convection anomaly presiding over India, an enhanced convection anomaly develops at the equator, and the cycle begins anew. The results of this regression indicate a mean oscillation period of about 35-45 days. The ISO is not exactly periodic, particularly during summer which results in a rapid decrease of correlations at long leads and lags.

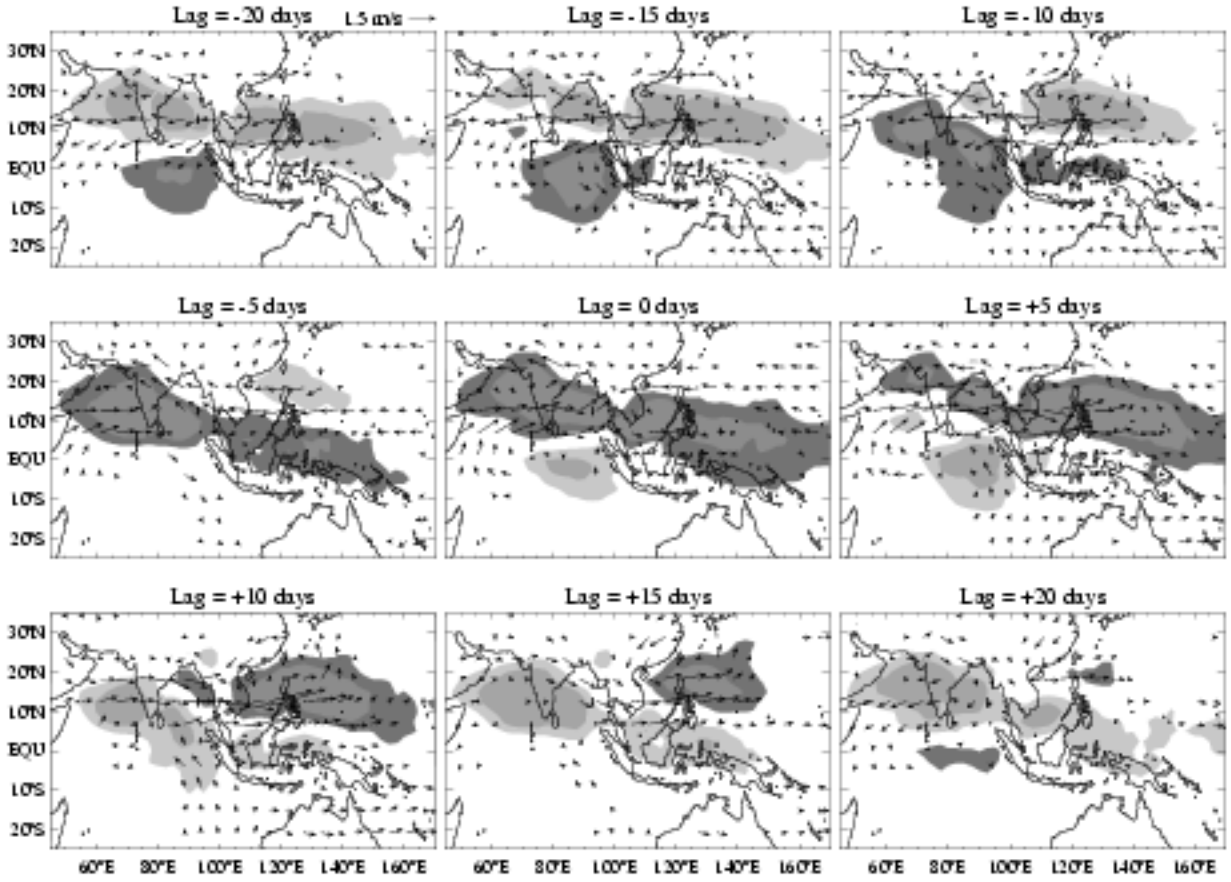

Figure 5.3. OLR (shaded) and 850-mb wind (vectors) perturbations associated with a 1 σ deviation in OLR_{25-80e} in the base region; 85°–90°E, 10°–15°N. The base region is regressed against data that is bandpass filtered to retain 25–80-day periods. Lagged regressions every 5 days between lag –20 days and lag +20 days are shown. Only locally significant OLR and wind vectors are plotted. Shading levels for OLR are every 3 W m^{-2}, dark shades indicate negative OLR anomalies, light shades indicate positive OLR anomalies.

5.3.2 Synoptic-Scale Westward Propagating Waves The wavenumber-frequency variance spectra (Fig. 5.2) identify a second important timescale in the Asian monsoon region, namely the high-frequency westward 5–10-day period spectral peaks. Figure 5.4 depicts lagged regression maps relative to a base region in the Bay of Bengal (85°–90°E, 12.5°–17.5°N) using OLR_{5-10w} as the predictor. As before, the results are not dependent on the position of the base region as long as it is located in the South Asian monsoon region within the area of maximum OLR_{5-10w} variance (approximately 10°–20°N, 70°–100°E, see Fig. 5.7a). For illustrative purposes, the base region is chosen to overlap the base region in the previous section. Lagged regressions are shown every two days from lag –2 days to lag +4 days. In addition to the regressed OLR and 850-mb winds, the regressed 850-mb relative vorticity is plotted with lined contours. The 850-mb level is selected since it is the level of the maximum relative vorticity response for these waves (Lau and Lau 1990). The dominant feature of Fig. 5.4 is the anticipated westward propagation of both the OLR anomalies and the associated low level cyclones and anticyclones. The evolution is reminiscent to that described by Lau and Lau (1990).

A relative vorticity perturbation first appears over the warm pool in the western Pacific ($\sim$130°E) and moves steadily westward towards the Indian subcontinent, reaching the Indian peninsula in about 10–12 days at a phase speed of $\sim$6 m s^{-1} . The characteristic period of these waves is about 6–8 days with a zonal wavelength of 4000–6000 km, corresponding to wavenumbers between 6 and 9. These estimates for period and wavenumber match the strong spectral peaks seen within the OLR_{5-10w} filter box in Fig. 5.2. The greatest negative point correlation is about –0.8, implying that these waves explain, at least locally, on the order of 60%

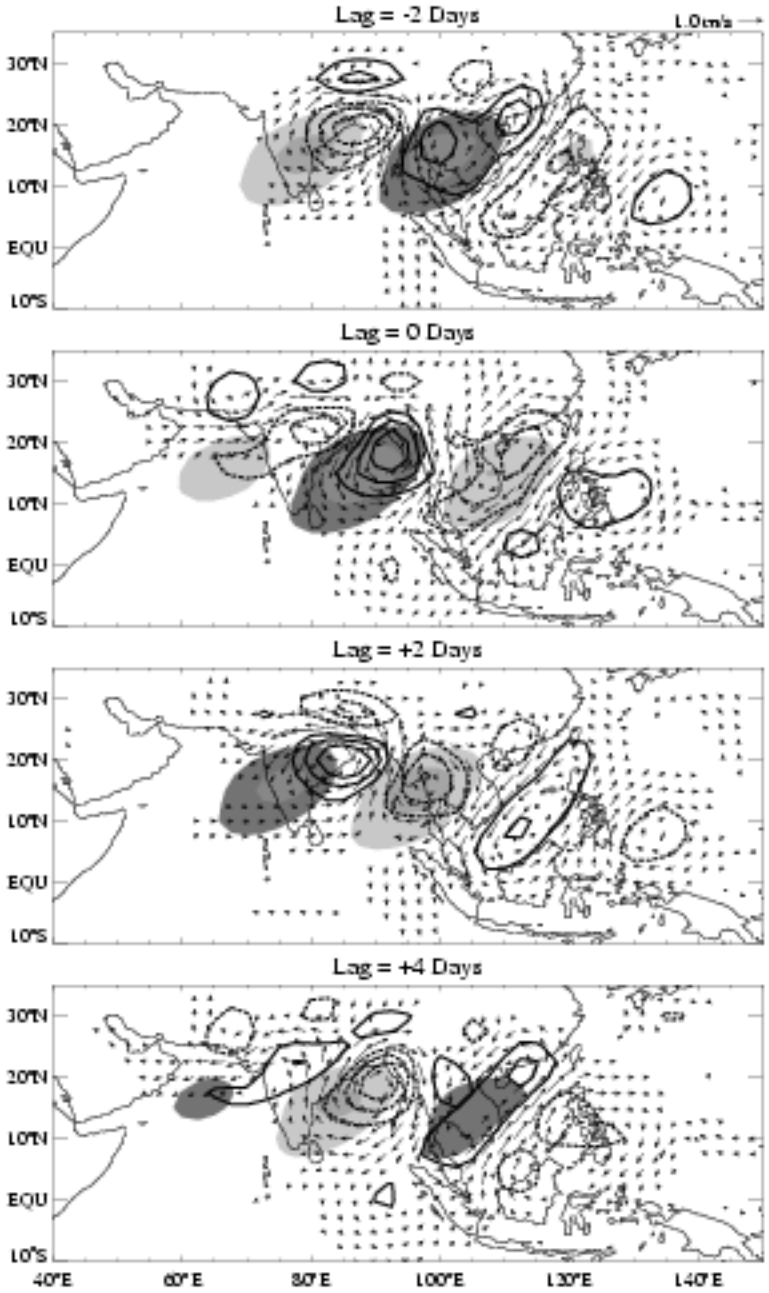

Figure 5.4. 5–10 day 850-mb wind (vectors), relative vorticity (contours), and OLR_{5-10w} (shaded) perturbations associated with a 1 σ standard deviation in OLR_{5-10w} in the base region; 85°–90°E, 12.5°–17.5°N. Lagged regressions between –2 and +4 days every 2 days are shown. Dark shades indicate negative OLR perturbations < -4 and -8 W m^{-2}, light shades indicate positive OLR perturbations $>$ +4 and +8 W m^{-2}. Only locally significant OLR and wind vectors are plotted. For clarity, relative vorticity is plotted everywhere regardless of significance. Relative vorticity contours are every 1 x 10^{-6} s^{-2} with the zero contour omitted.

of the variance in the 5–10-day westward 4 to 12 zonal wavenumber band. Lau and Lau (1990) point out that the sites of active transient activity that they identify in their study are also well known as source regions for other cyclonic weather systems such as monsoon depressions in the Bay of Bengal and typhoons in the western Pacific. It is possible that such disturbances develop from strong episodes of these synoptic-scale wavy disturbances as suggested by Saha *et al.* (1981) and Krishnamurti *et al.* (1977). In fact, the low-level wind response to convection shown in Fig. 5.4 strongly resembles that of the monsoon depressions identified in the comprehensive Kiladis and Weickmann (1997) study of submonthly tropical convection; that is, the convection is embedded in westerlies and cross-equatorial flow into the convection from the winter hemisphere is also present.

5.3.3 Synoptic-Scale Waves and the ISO Phase A primary goal of this chapter is to evaluate the interaction between the two dominant modes of intraseasonal variability during the summer monsoon, namely, the ISO and westward propagating synoptic-scale waves. As noted in the introduction, each individual ISO convective system is made up of many higher frequency disturbances from synoptic to mesoscale. As is apparent in Fig. 5.1, high-frequency wave activity in the Indian monsoon region is not restricted to times when the ISO is in its convective phase. The question is, what differences, if any, are observed between those synoptic-scale systems that are present during the ISO convective phase and those that are present during the ISO suppressed phase?

To begin to answer this question, two separate linear regressions are completed, focusing in turn on synoptic-scale wave activity during the convective and suppressed phases of the ISO. The convective phase of the ISO is defined simply as all days when the area-average OLR_{25-80E} is one-standard-deviation or more below

the JJAS mean OLR_{25-80e} in the Indian monsoon region (70°–85°E, 10°–20°N). A lagged cross-correlation and linear regression analysis is subsequently performed using area-averaged Bay of Bengal OLR_{5-10w} data during the selected dates as the predictive timeseries. In a similar manner, OLR_{5-10w} in the base region is used as the predictor for dates during the ISO suppressed phase in the Indian monsoon region.

The results of the two lagged regressions are shown as time-longitude sections along 15°N in Fig. 5.5a (convective ISO phase) and Fig. 5.5b (suppressed ISO phase). The synoptic-scale waves during the opposite phases of the ISO are identical for the most part with both exhibiting phase speeds relative to ground of about 8 m s^{-1} or 7° per day, periods of approximately 6-8 days, and westward wavenumbers in the 6 to 9 range. Low level cyclones and anticyclones (not shown), similar to those shown in Fig. 5.4, are also seen during both ISO phases. The only major difference between the two phases is the longitudinal span over which an individual convection event travels during its lifetime. During the convective ISO phase, the average high-frequency convective wave originates at around 110°–120°E in the South China Sea and propagates west to the Bay of Bengal and finally reaching on the west coast of India about 8 to 10 days after the convection first developed in the South China Sea. The disturbances that occur during the suppressed phase of the ISO develop about 20° further east at 130°–140°E. These synoptic-scale waves also propagate westward into the Indian monsoon region, generating significant precipitation over the Indian subcontinent during the suppressed ISO or break phase of the monsoon.

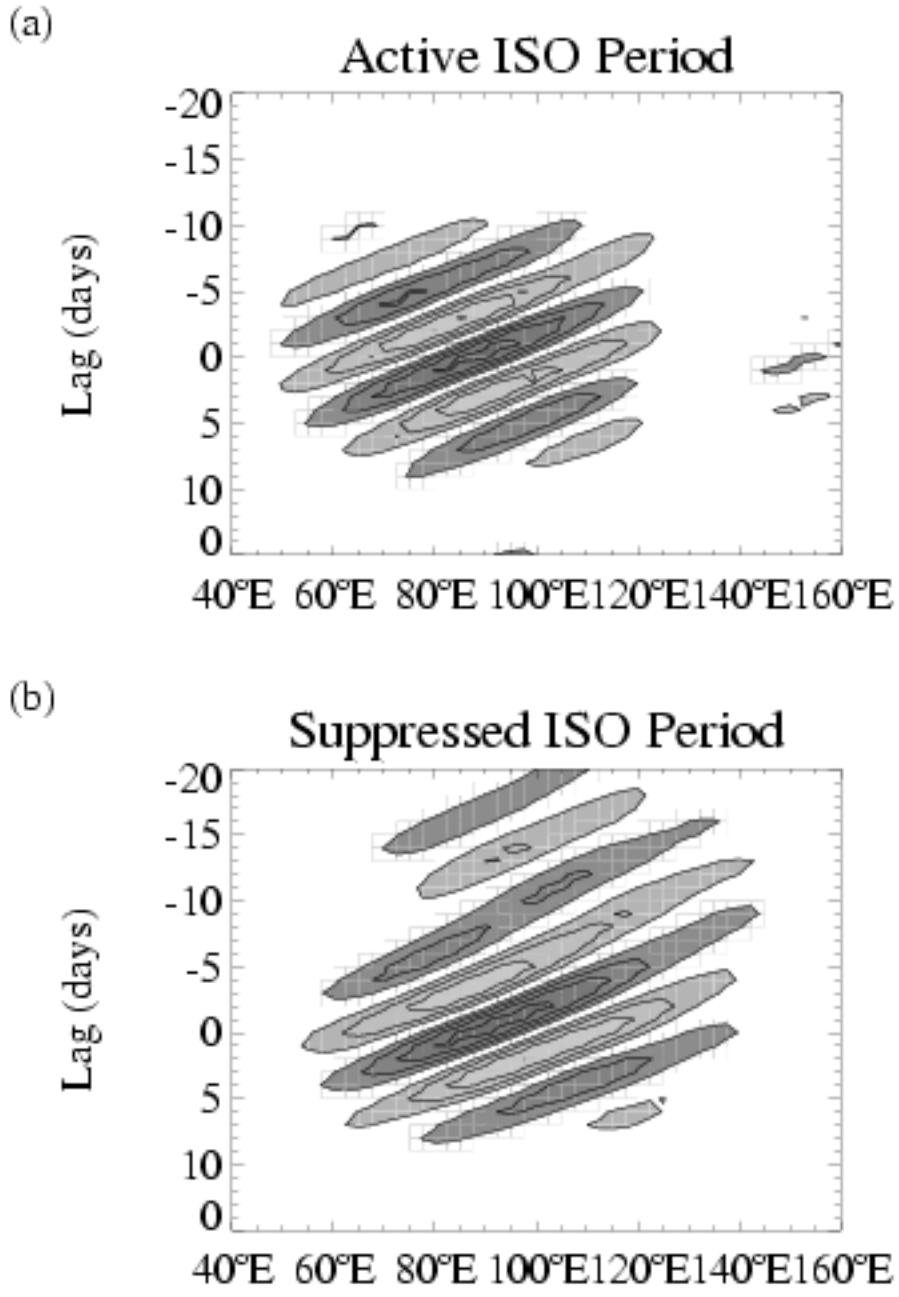

Figure 5.5. Lag-longitude sections of OLR_{5-10w} regression results along 15°N. Two separate lagged regressions are completed for times when OLR_{25-80e} over Indian subcontinent (70°–85°E, 10°–20°N) is (a) $<-1\ \sigma$ from the mean (active period) and (b) $> 1\ \sigma$ from the mean (break period). Contour levels are every 3 W m^{-2}, dark shades indicate negative OLR_{5-10w} anomalies, light colors indicate positive OLRW anomalies.

5.4 Synoptic-Scale Wave Activity and ISO

5.4.1 Measure of Synoptic-Scale Wave Activity In order to investigate the relationship between the high-frequency synoptic-scale waves and the slowly varying ISO, a measure for the synoptic-scale transient activity is required. The measure used here is wavelet derived variance which is generated according to the method outlined by Torrence and Compo (1998) and is described briefly here. First, at each grid point, the wavelet transform is computed for the entire record timeseries (1975-1997) of the wavenumber-frequency filtered OLR_{5-10w} timeseries using the Morlet wavelet basis. Second, the wavelet variance spectrum is calculated at each grid point. Finally, the wavelet variance spectrum is averaged over the desired range of scales generating a timeseries of OLR_{5-10w} variance at a single grid point. This procedure is repeated for each grid point resulting ultimately in a global OLR_{5-10w} variance dataset at the 2.5° x 2.5° spatial resolution of the original OLR data. Henceforth, this variance dataset will be denoted as $OLR_{5-10w}{}^2$. The advantage of wavelet-derived variance as opposed to squaring bandpass-filtered data is that each individual scale is analyzed with a window appropriate for that individual scale (Lau and Weng 1995). A secondary advantage of wavelet-derived variance is that, since the variance timeseries are chi-squared distributed, the significance of each point in the timeseries can be assessed relative to red noise or some other background spectrum (Compo 1997).

The utility of such a measure of wave activity is illustrated in Figs. 5.6a and b. Figure 5.6a shows the timeseries of OLR_{5-10w} and $OLR_{5-10w}{}^2$ at a single grid point in the Bay of Bengal (90°E, 15°N) for June and July, 1992. As the amplitude of OLR_{5-10w} fluctuations increases during the second week of July, the OLR_{5-10w} variance increases accordingly. A time-longitude section of OLR_{5-10w} along 15°N,

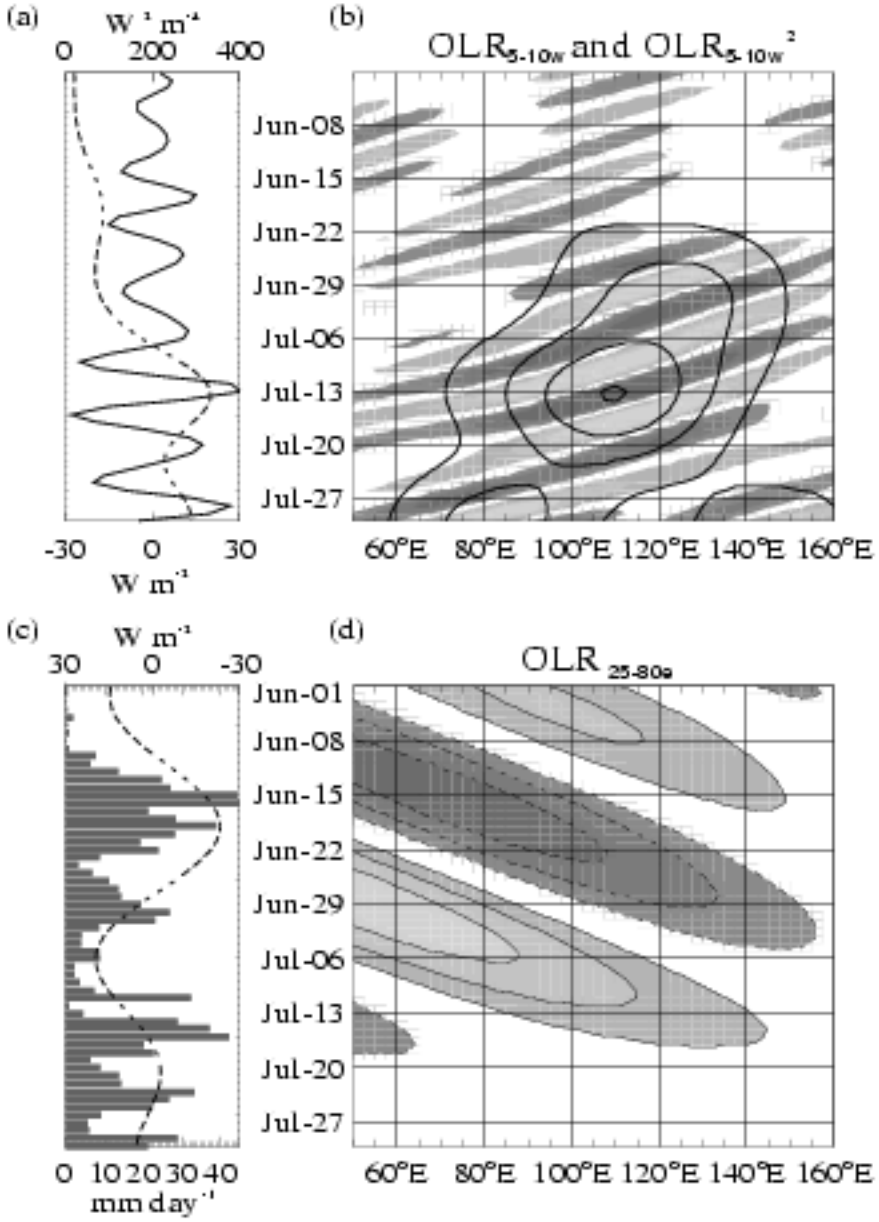

Figure 5.6. OLR_{5-10w}, $OLR_{5-10w}{}^2$, and OLR_{25-80e}, and precipitation for June to July 1992. (a) OLR_{5-10w} (solid line) and $OLR_{5-10w}{}^2$ (dashed line) at 90°E, 15°N. (b) Time-longitude section of OLR_{5-10w} (shaded contours) and $OLR_{5-10w}{}^2$ (lined contours) along 15°N. (c) Precipitation (bars) and OLR_{25-80e} (dashed line) at 90°E, 15°N 85°–90°E, 15°–20°N. (d) Time-longitude diagram of OLR_{25-80e} along 15°N. Dark shades indicated negative OLR anomlies, light shades indicate positive OLR anomalies, contour interval is 7.5 W m^{-2} with the zero contour omitted. $OLR_{5-10w}{}^2$ contour interval is 150 W^2 m^{-4}.

corresponding to the same time frame, is shown in Fig. 5.6b. The amplitude of the westward propagating convective disturbances (shaded contours) show clear spatial and temporal variability. The waves can sometimes be quite long-lived. For example, a single convective disturbance can be tracked all the way from 150°E starting on July 6, finally dissipating around 60°E fourteen days later. Figure 5.6c is a histogram of precipitation in addition to the OLR_{25-80e} timeseries at the same Bay of Bengal grid point as in Fig. 5.6a, while Fig. 5.6d is a time-longitude diagram of OLR_{25-80e}. An active period of rainfall dominates through the middle of June followed by a break period at the beginning of July, roughly in accordance with the OLR_{25-80e} timeseries. Individual peaks in precipitation are often coincident with the passing of synoptic-scale convective disturbances, e.g. compare sign of OLR_{5-10w} at 90°E in Fig. 5.6b with amplitude of precipitation in Fig. 5.6c on June 30, July 10, and July 16. Overplotted with solid lined contours in Fig. 5.6b is the time-longitude diagram of $OLR_{5-10w}{}^2$. This figure is a "power Hovmöller diagram" (defined by Torrence and Compo 1998) which describes the temporal and zonal evolution of westward manifold variance at scales between 5 and 10 days. The increase in variance at 120°–150°E during the last week of June reflects the increase in waviness in OLR_{5-10w} that occurs during that time period. An interesting feature of the power Hovmöller diagram is the westward movement of enhanced variance during the middle of the period. The westward evolution of variance begins subsequent to the arrival of ISO convection in the western Pacific Ocean.

Peaks in $OLR_{5-10w}{}^2$ occur during both the active and suppressed ISO phases in the Indian monsoon region. In the box 85°–90°E, 12.5°–17.5°N in the central Bay of Bengal, 41 statistically significant $OLR_{5-10w}{}^2$ peaks are identified

during the 19 summers surveyed in this study. Twenty-four of them occur during the wet ISO phase, while the 17 remaining episodes happen during the dry ISO phase. The relationship between the ISO and the synoptic-scale disturbances will be examined through two separate composite analyses of synoptic-scale wave activity during active and break periods in Sections 5.4.2 and 5.4.3, respectively.

The JJAS climatology of $OLR_{5-10w}{}^2$ is shown in Fig. 5.7a along with the JJAS climatological zonal vertical wind shear ($u_{200} - u_{850}$) in Fig. 5.7b. The region of high $OLR_{5-10w}{}^2$ is largely coincident with the area of easterly vertical wind shear. The easterly vertical wind shear in the Asian monsoon region reflects the mean opposite flow of the upper level easterly jet and the low level southwesterly monsoon flow. Wang and Xie (1996) and Webster and Chang (1997) found in modeling studies that an easterly shear confines equatorially trapped baroclinic Rossby waves to the lower troposphere. The synoptic-scale waves that make up the $OLR_{5-10w}{}^2$, introduced in Section 5.3.2, exhibit much stronger signals at low levels relative to upper levels. Xie and Wang (1996) found, in a companion study to Wang and Xie (1996), that an easterly vertical wind shear in the presence of moisture convergence and induced heating destabilizes equatorial Rossby waves with wavelengths of about 3000 to 5000 km (wavenumbers 8 to 13).

The mean annual cycles of $OLR_{5-10w}{}^2$ and the zonal vertical wind shear in the Bay of Bengal and the western Pacific Ocean are shown in Fig. 5.7c. Especially in the Bay of Bengal, the annual cycle of $OLR_{5-10w}{}^2$ mirrors that of the zonal vertical wind shear with synoptic-scale wave activity developing shortly after the monsoon flow generates an easterly vertical wind shear in early June and degrading as the monsoon degenerates in October. In the western Pacific Ocean, the mean easterly vertical wind shear is not nearly as strong during the summer months as it

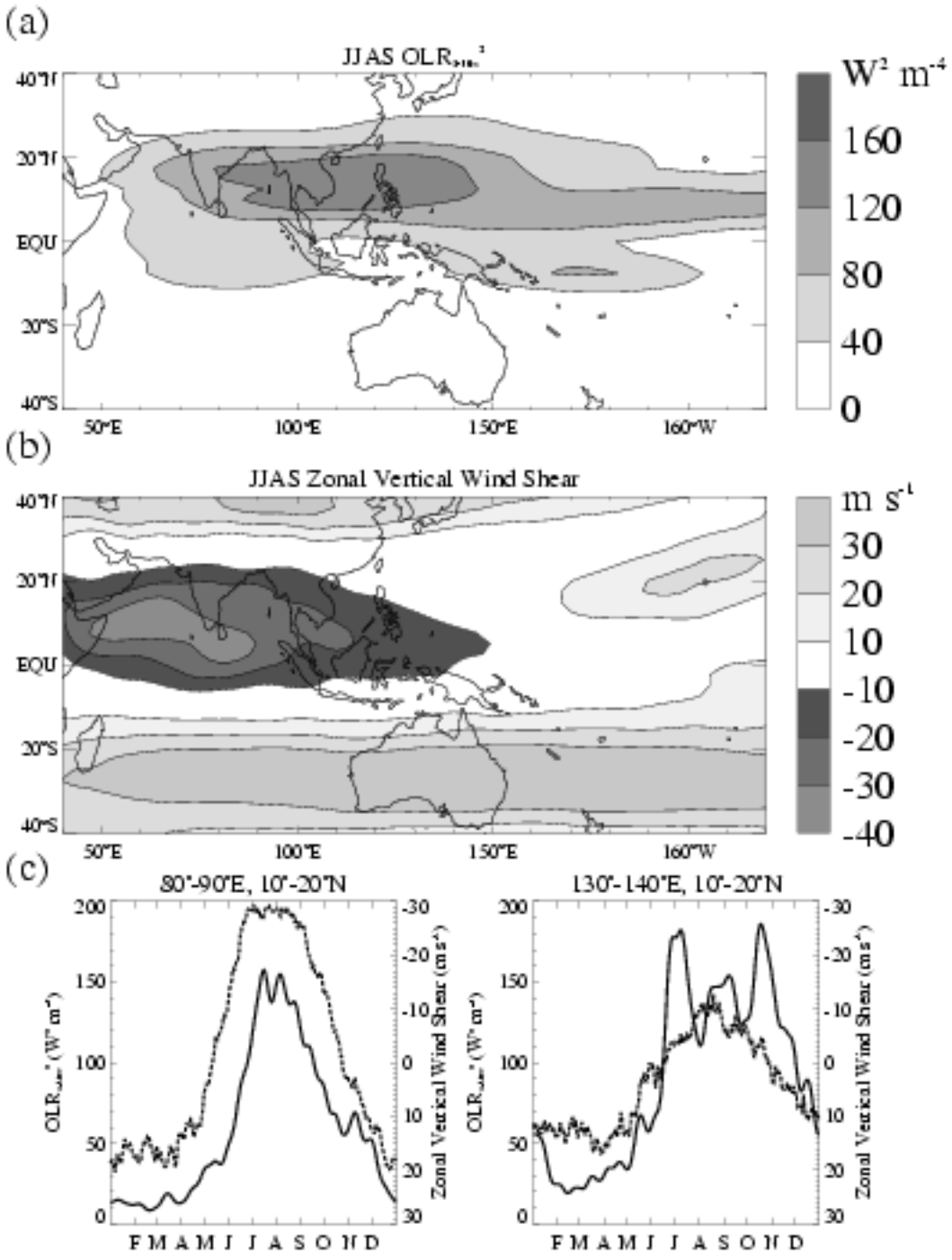

Figure 5.7. Climatology for JJAS, 1975–1997, of (a) $\mathrm{OLR}_{5-10w}{}^2$ and (b) zonal vertical wind shear ($u_{200} - u_{850}$). (c) Mean annual cycle of $\mathrm{OLR}_{5-10w}{}^2$ (solid line) and zonal vertical wind shear (dashed line) in Bay of Bengal and western Pacific Ocean.

is over the Bay of Bengal. In addition, the OLR_{5-10w} variance remains high from June through November, coinciding with the main tropical cyclone season in the northwest Pacific Ocean basin.

5.4.2 Active ISO Phase First, the relationship between synoptic-scale wave activity and the active ISO convection in the Indian monsoon region is investigated. The active ISO phase is defined here as time-periods when OLR_{25-80e} over the Bay of Bengal (10°–15°N, 85°–90°E) is greater than 0.5σ below the summertime mean value of OLR_{25-80e} in this region (approximately zero by construction). By this method, 48 active periods are identified over the nineteen summers included in this study, corresponding to about 2.5 events per summer.

Lagged composites of anomalous ${OLR_{5-10w}}^2$ and OLR_{25-80e} are completed where day zero is defined as the day during which the Bay of Bengal OLR_{25-80e} is minimum. Lagged maps of the composited OLR_{25-80e} and ${OLR_{5-10w}}^2$ anomalies are shown every 4 days for lags –12 days to lag +8 days in Fig. 5.8. Only regions where the ${OLR_{5-10w}}^2$ anomaly exceeds the 90% significance level are contoured. The significance level is determined according to the method outlined by Compo (1997) and briefly summarized here. The d.o.f. of the composite OLR_{5-10w} variance are calculated directly by multiplying the number of composite events by the averaged-in-scale d.o.f. (Torrence and Compo 1998). The background variance is obtained by compositing the seasonal cycle of ${OLR_{5-10w}}^2$ for the same dates as the ${OLR_{5-10w}}^2$ composite. The composite of the ${OLR_{5-10w}}^2$ seasonal cycle, then, is the background variance to which the ${OLR_{5-10w}}^2$ is compared with an upper and lower confidence interval that is determined by the d.o.f.. Composited ${OLR_{5-10w}}^2$ values, at any lag, that are greater than the upper limit or less than the lower limit are considered statistically significant. Figure 5.9a is an example of how the statistical

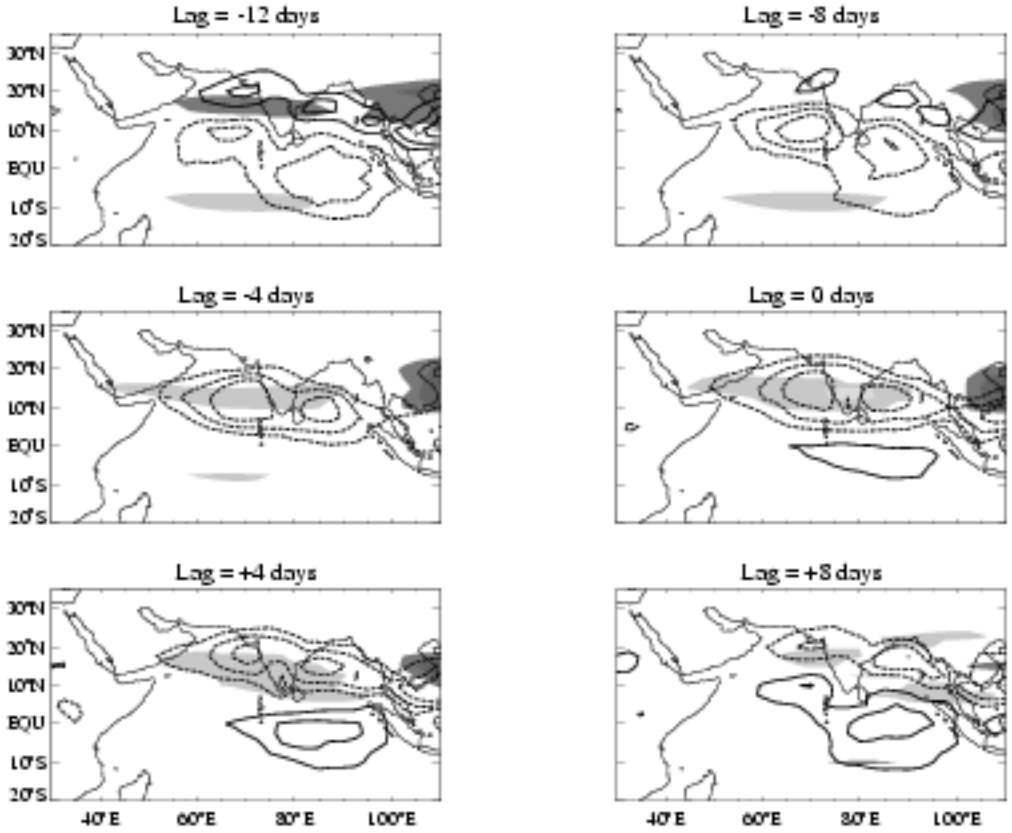

Figure 5.8. Lagged maps of composited OLR_{25-80e} (contours) and anomalous $OLR_{5-10w}{}^2$ (shaded). Lagged composites are compiled relative to summertime minimums of OLR_{25-80e} at 85°–90°E, 10°–15°N. A total of 48 events are composited. Contour intervals for $OLR_{5-10w}{}^2$ are every 10 W^2 m^{-4} with light shades indicating anomalously high $OLR_{5-10w}{}^2$ and dark shades indicating anomalously low $OLR_{5-10w}{}^2$. Only areas that are statistically significant at the 90% level are contoured (see text for details). OLR_{25-80e} contours are every 5 W m^{-2} with lined contours indicating suppressed convection and dashed contours indicating enhanced convection.

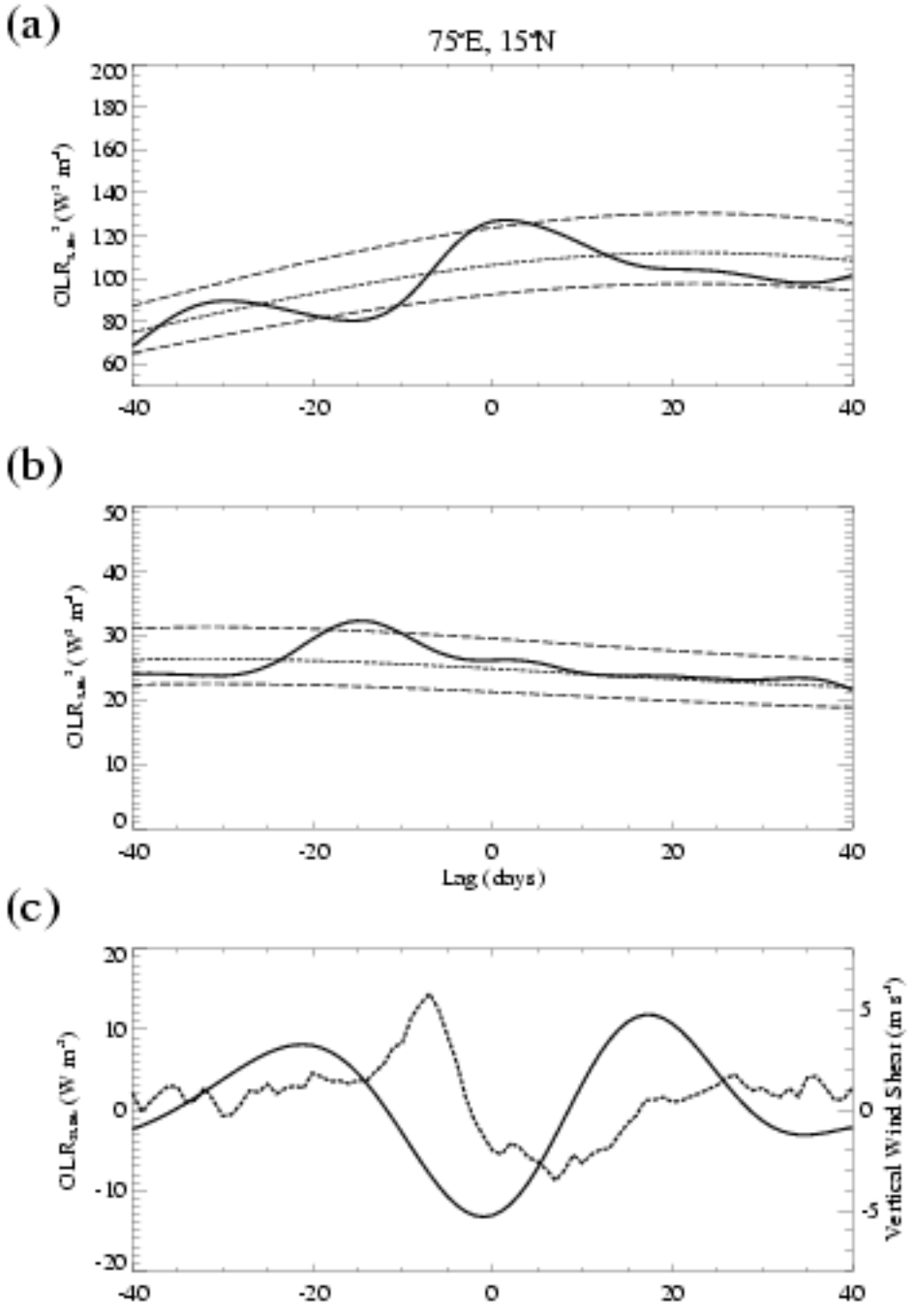

Figure 5.9. Lagged timeseries at 75°E, 15°N of composites based on OLR_{25-80e} minimums at 85°–90°E, 10°–15°N. (a) $OLR_{5-10w}{}^2$ (solid), composite $OLR_{5-10w}{}^2$ seasonal cycle (short dash), and $OLR_{5-10w}{}^2$ 90% confidence intervals (long dash). (b) Same as (a) except for $OLR_{5-10e}{}^2$. (c) OLR_{25-80e} and zonal vertical wind shear ($u_{200}-u_{850}$).

significance test is applied at an individual grid point along the west coast of India (75°E, 15°N). At and around lag zero days the $OLR_{5-10w}{}^2$ value exceeds the upper confidence limit. Similarly, at lag –15 days, the $OLR_{5-10w}{}^2$ value is less than the lower confidence limit indicating that the OLR_{5-10w} variance is below normal at that lag at a statistically significant level. The 30–40-day nature of the ISO is seen as a return to above normal variance at lag –30 to –35 days although this variance peak is not statistically significant.

The composite evolution of ISO convection (lined contours in Fig. 5.8) is generally analogous to the results from the lagged cross-correlation and linear regression analysis presented in Fig. 5.3 with ISO convection at the equator preceding convection at Indian subcontinent latitudes. By lag -4 days at 10°–15°N, there is a statistically significant positive $OLR_{5-10w}{}^2$ anomaly that is roughly coincident with the northward propagating ISO convective signal. The positive $OLR_{5-10w}{}^2$ anomaly remains until the ISO convection dissipates at lag +8 days. Clearly, the composite results support the notion that the westward propagating disturbances are excited during the northward progression of the ISO.

While Fig. 5.8 implies that OLR variance is modulated by the active ISO phase, the composite results alone do not prove definitively that synoptic-scale westward propagating waves are excited selectively relative to other convection frequencies. Large-scale convective envelopes modulate synoptic-scale convection at all frequencies (Hendon and Liebmann 1994; Kiladis *et al.* 1994; Meehl *et al.* 1996), not just those in the OLR_{5-10w} band evaluated here. The question is whether or not the westward propagating 5–10-day waves that are monitored here are excited preferentially by the physical mechanism proposed by Lau and Peng (1990). To evaluate this, the OLR data is wavenumber-frequency filtered in

the same manner described in Section 5.2.3 to eastward wavenumbers 4 to 10 with periods of 5 to 10 days. A variance dataset ($OLR_{5-10e}{}^2$) then is calculated and subsequently composited about the same active period dates as delineated above. Figure 5.9b shows the results of the $OLR_{5-10e}{}^2$ composite at 75°E, 15°N. At lag 0 days, when the OLR_{5-10w} variance is high (Fig. 5.9a), the OLR_{5-10e} variance is approximately normal. The $OLR_{5-10e}{}^2$ exhibits no evidence of modulation by the 30–40-day oscillation that would be apparent as a 30–40-day oscillation in the lagged $OLR_{5-10e}{}^2$ composite.

To pursue further the question of whether or not the 5–10-day westward propagating waves are excited preferentially during the wet phase of the ISO over India, two Fourier spectral analyses are completed during active and suppressed ISO periods separately. Frequency spectra are calculated on 31-day OLR anomaly time-series (tapered to zero at endpoints) centered at the minimum (active) and maximum OLR_{25-80e} dates at all grid points in the Bay of Bengal (80°–90°E, 10°–20°N). The average variance spectrum over all the grid points is calculated for both the wet and dry period variance spectra and is normalized by the total variance at periods less than 10 days. The wet to dry period variance ratio is shown in Fig. 5.10a. Variance ratio values greater than one indicate spectral frequencies at which the active ISO period spectral variance exceeds the suppressed ISO period spectral variance. For most of the spectrum, the variance ratio is near one, except at a period of approximately 6 days, where the variance ratio is nearly 1.3, indicating that during the active phase of the ISO over the Bay of Bengal the 6 day variance is approximately 30% greater than during the suppressed phase. A similar spectral analysis is completed for the equatorial Indian Ocean (80°–90°E, 5°S–5°N) and is shown in Fig. 5.10b. At the equator, the variance ratio is reasonably close to one at all periods except between

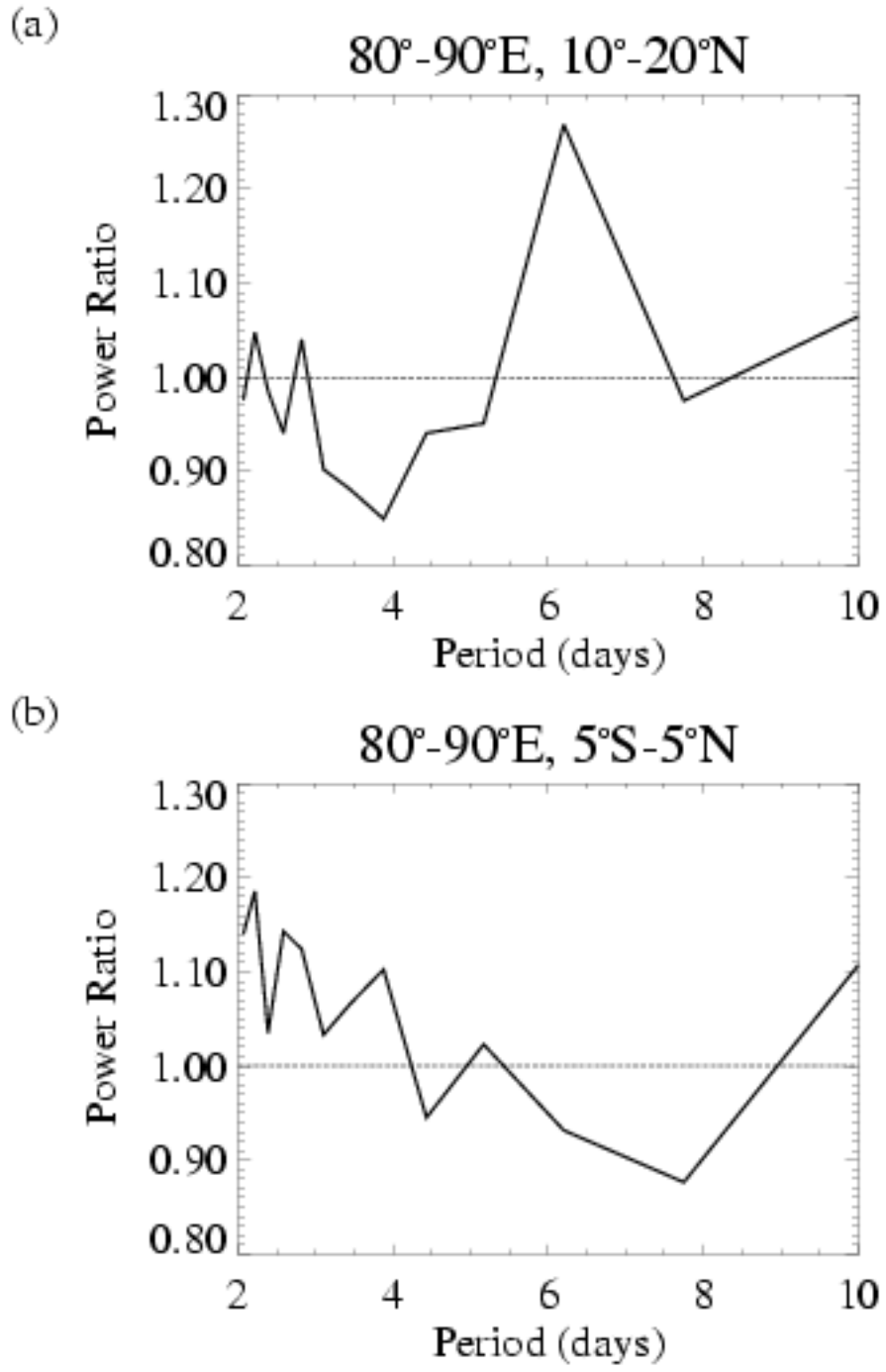

Figure 5.10. Ratio of OLR power spectra calculated during convective phase of ISO relative to power spectra calculated during suppressed phase. Spectra are calculated from 31-day OLR anomaly timeseries centered about a minimum (convective) or a maximum (suppressed) in summertime OLR_{25-80e} at all grid points inclusive in (a) 70°–90°E, 10°–20°N and (b) 70°–90°E, 5°S–5°N.

2–2.5 days, a result that is consistent with the spectral analysis done by Hendon and Liebmann (1994). The conclusion, therefore, is that the increase in OLR_{5-10w} variance during the wet phase of the ISO over the Asian monsoon domain is not simply a product of increased OLR variance at all frequencies, but instead represents a modulation or excitation of the westward propagating synoptic-scale waves, possibly via the interaction between the equatorial heating and the large scale easterly vertical wind shear. An important caveat is provided by Liebmann *et al.* (1994) in their study of tropical cyclone and tropical storm initiation. Liebmann *et al.* (1994) show that cyclones tend to occur more often during the wet phase of the ISO, which is in support of the results of this study. However, they also find that the increase in tropical storms during the wet phase of the ISO is not due to a predilection of tropical storms to the dynamical environment of the wet phase of the ISO, but instead simply indicates a preference for presence of any slowly varying convection, not necessarily that connected to the ISO. Of course, in the Indian monsoon region, ISO timescale convection dominates the low-frequency spectrum.

5.4.3 Suppressed ISO Phase Synoptic-scale wave activity in the Bay of Bengal is not restricted to active periods of the monsoon. On 17 occasions between 1975 and 1997, strong westward propagating wave activity, as determined by high $OLR_{5-10w}{}^2$ values, is observed during the suppressed ISO phase. As suggested in Fig. 5.5b, the source region of synoptic-scale disturbances during a break phase of the Indian monsoon may be located outside the Indian monsoon domain in the western Pacific Ocean. This hypothesis is tested here by generating a lagged composite of $OLR_{5-10w}{}^2$ and OLR_{25-80e} centered about the 17 statistically significant $OLR_{5-10w}{}^2$ peaks that occur during the suppressed ISO phase in the Bay of Bengal. The composite result is shown as a time-longitude diagram in Fig. 5.11.

OLR_{5-10w} variance increases to above normal values at 110°–140°E subsequent to the arrival of the convective phase of the ISO in the same region. After an initial intensification of OLR_{5-10w} variance, the region of high $OLR_{5-10w}{}^2$ moves westward towards the Indian subcontinent, propagating at a rate of approximately 6–7 m s^{-1}, approximately the same propagation speed of individual synoptic-scale waves. The composited OLR_{5-10w} variance remains above normal over India for about 10–12 days, time enough for about 1–2 westward propagating synoptic-scale systems to pass through the region.

In the composite results, the synoptic-scale wave activity at 110°–120°E appears to be modulated by ISO convection at the same longitude. The result is not conclusive since compositing relative to high $OLR_{5-10w}{}^2$ periods that occur during *suppressed* ISO periods over India dictates to some degree the OLR_{25-80e} composite results. To examine the robustness of the apparent modulation of synoptic-scale wave activity by the ISO in the western Pacific Ocean, OLR_{25-80e} and $OLR_{5-10w}{}^2$ are composited in the same manner as in Section 5.4.2, except OLR_{25-80e} is used to identify 36 strong ISO convection events in the western Pacific Ocean (125°–130°E, 10°–15°N). Lagged composite maps (Fig. 5.12) indicate that $OLR_{5-10w}{}^2$ is modulated by ISO convection, but the synoptic-scale wave activity requires time to develop as explained below. At lag zero days, when the ISO convection is at a maximum in the base region, $OLR_{5-10w}{}^2$ values are near normal. It is not until lag +4 days to lag +8 days that synoptic-scale westward propagating wave activity fully develops, after which time it remains high through lag +20 days, well after the ISO convection has dissipated. The lag between the ISO convection maximum and the $OLR_{5-10w}{}^2$ maximum may be at least partly attributed to the timing of the zonal vertical wind shear anomaly associated with the ISO. As noted earlier, an

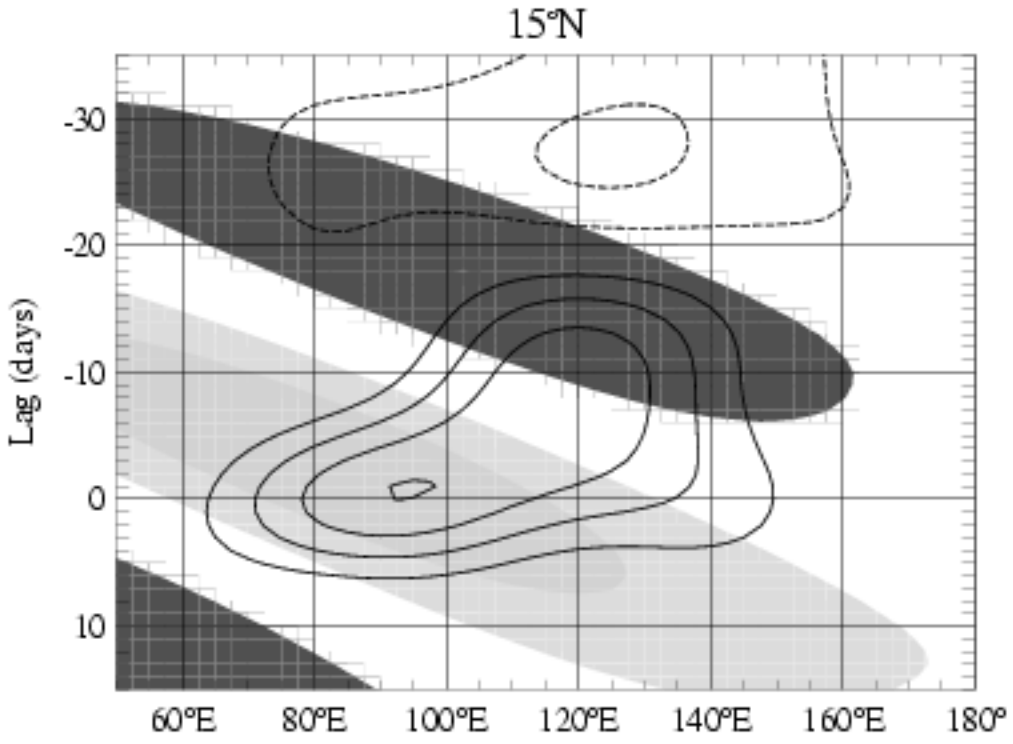

Figure 5.11. Lag-longitude diagram of composited $OLR_{5-10w}{}^2$ anomalies (contours) and OLR_{25-80e} (shaded) at 15°N. Lagged composites are compiled relative to maximums of $OLR_{5-10w}{}^2$ in central Bay of Bengal. Only $OLR_{5-10w}{}^2$ maximums that are significant at the 90% level and occur during the suppressed phase of the ISO are considered yielding a total of 17 events that go into the composite. Contour intervals for $OLR_{5-10w}{}^2$ anomalies are every 30 W^2 m^{-4} with the zero contour omitted. Contour intervals for OLR_{25-80e} are every 3 W m^{-2}, dark shades indicating negative OLR_{25-80e} anomalies and light shades indicating positive OLR_{25-80e} anomalies.

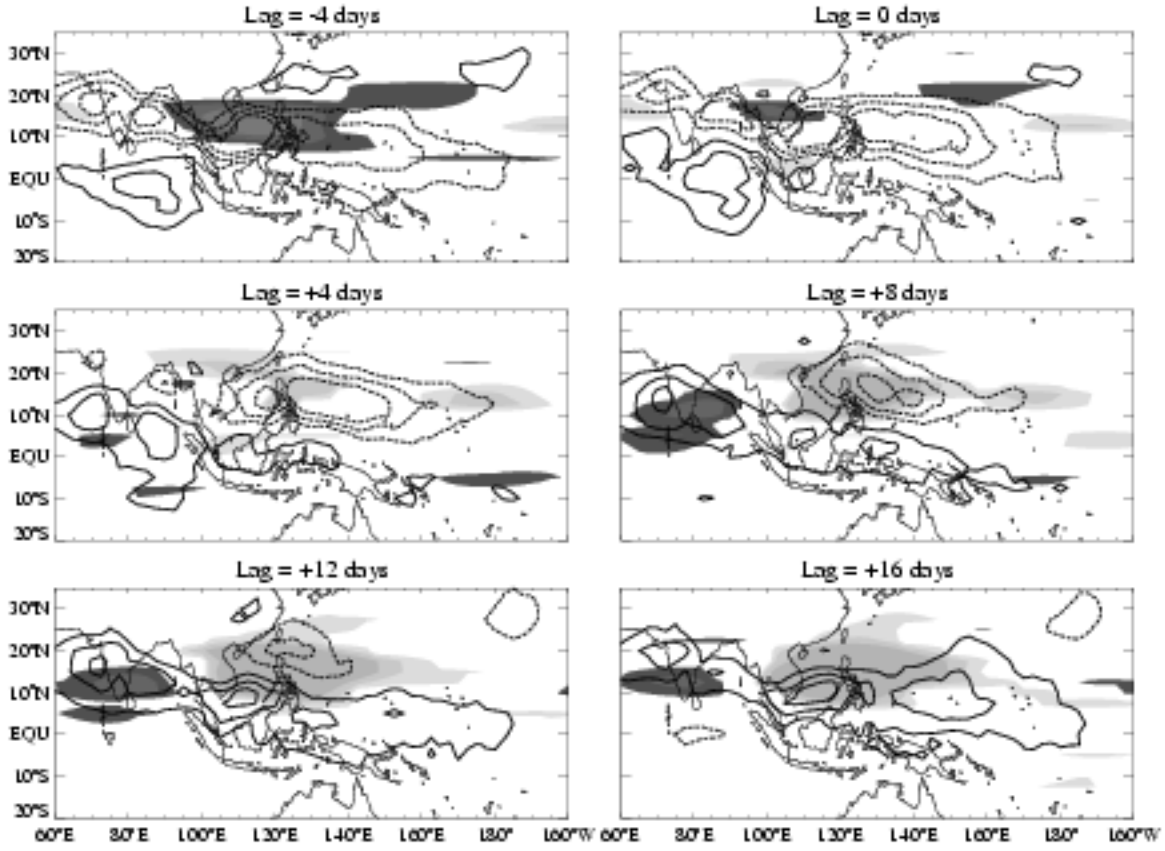

Figure 5.12. Lagged maps of composited OLR_{25-80e} (contours) and anomalous $OLR_{5-10w}{}^2$ (shaded). Lagged composites are compiled relative to summertime minimums of OLR_{25-80e} at 125°–130°E, 10°–15°N. A total of 36 events are composited. Contour intervals for $OLR_{5-10w}{}^2$ are every 10 W^2 m^{-4} with light shades indicating anomalously high $OLR_{5-10w}{}^2$ and dark shades indicating anomalously low $OLR_{5-10w}{}^2$. Only areas that are statistically significant at the 90% level are contoured (see text for details). OLR_{25-80e} contours are every 5 W m^{-2} with lined contours indicating suppressed convection and dashed contours indicating enhanced convection.

easterly vertical wind shear generates an instability when coupled with convective heating at wavelengths similar to the synoptic-scale waves studied here (Xie and Wang 1996). In the Bay of Bengal, there is no lag between the ISO convection and the increase in synoptic-scale wave activity because a strong easterly vertical wind shear is an inherent feature of the climatological basic state. However, the summertime climatological easterly vertical wind shear is comparatively weaker by 10 to 20 m s^{-1} over the western Pacific Ocean (see Fig. 5.7). Therefore, the easterly vertical wind shear anomaly of –15 m s^{-1} that lags the ISO convection by about 10–12 days (see Fig. 5.13c) may play a critical role in determining the timing of synoptic-scale wave excitement over the western Pacific Ocean. As seen in Fig. 5.13a, the $OLR_{5-10w}{}^2$ rises to above normal values at about the same time that the easterly vertical wind shear anomaly maximizes.

It is important to note that the lagged composite maps in Fig. 5.12 do not indicate westward propagation of synoptic-scale wave activity. This result seems contrary to the composite result presented in Fig. 5.11 that says that synoptic-scale wave activity does move westward from the western Pacific Ocean during a break period. The results shown in Fig. 5.11 represent a composite based only on the 17 occasions when an anomalous $OLR_{5-10w}{}^2$ peak occurs during a suppressed ISO period over India. Thirty-six total suppressed periods are identified which means that only about half of the suppressed periods over India are marked by synoptic-scale wave activity. This observation lead us to question whether or not propagation from the western Pacific Ocean across southeast Asia to the northern Indian Ocean is dependent on a basic state that supports propagation of synoptic-scale waves. To test this hypothesis, the maximums of $OLR_{5-10w}{}^2$ over the western Pacific Ocean are separated into two categories; those that were and were not followed by maximums

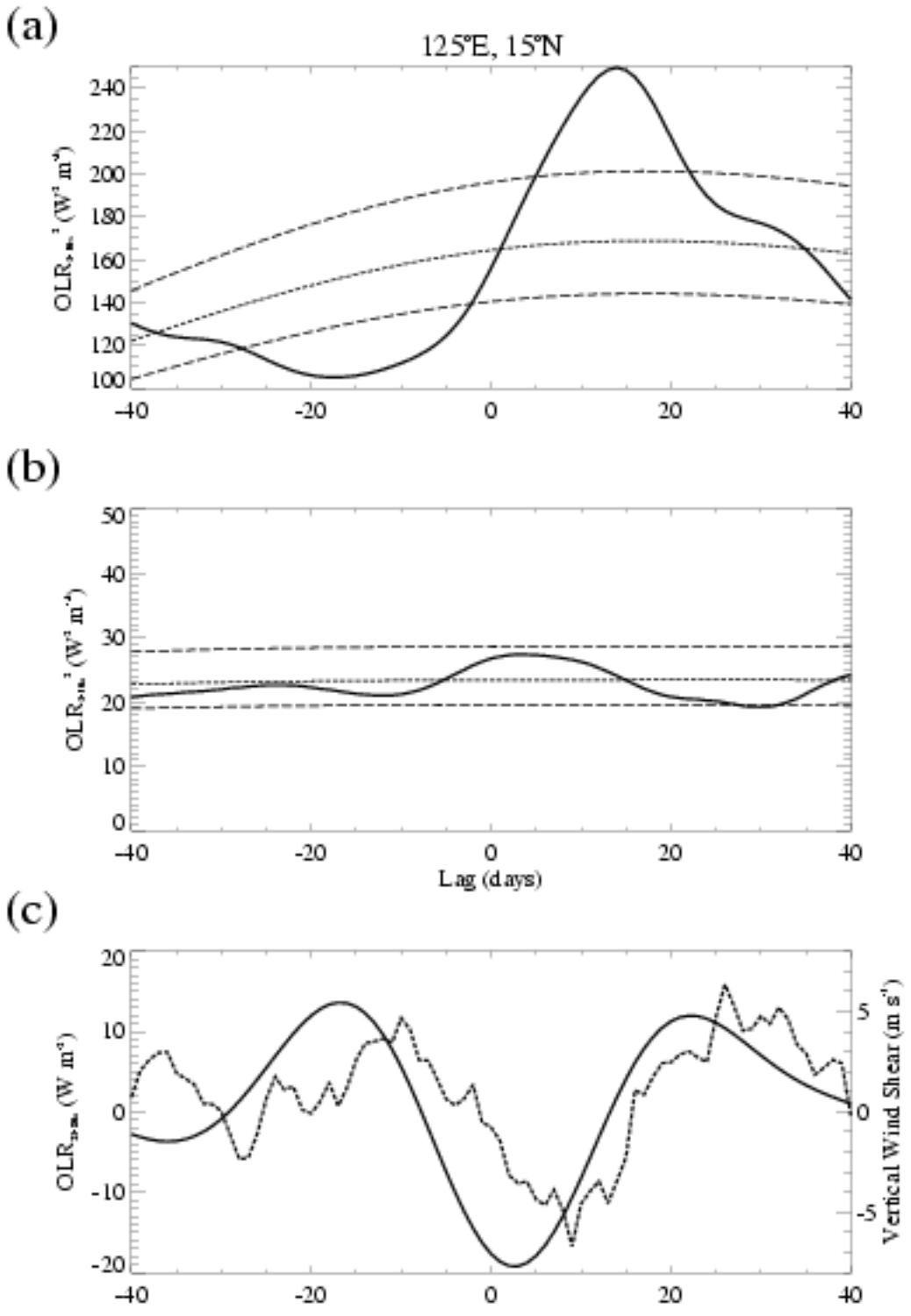

Figure 5.13. Same as in Fig. 5.9 except for lagged timeseries at 125°E, 15°N, composited based on minimums of OLR_{25-80e} at 125°–130°E, 10°–15°N.

of $OLR_{5-10w}{}^2$ over the Bay of Bengal. Of the 43 statistically significant summertime $OLR_{5-10w}{}^2$ peaks in the western Pacific Ocean, 17 were followed by synoptic-scale wave activity over India while 26 were not. Maps of composite lower level winds and zonal vertical wind shear for the 20 days after an $OLR_{5-10w}{}^2$ peak in the western Pacific Ocean are shown in Fig. 5.14. Both cases feature the strong monsoonal flow that dominates the circulation at this time of year. There does not appear to be major differences in the circulation between the cases. The only clearly distinguishable difference is an enhanced easterly vertical wind shear north of 15°N across southern China when westward movement of OLR_{5-10w} variance is detected. It is possible that the enhanced easterly vertical wind shear traps the synoptic-scale waves closer to the equator thus acting as a wave guide that directs the synoptic-scale waves across southeast Asia and onto the Indian peninsula.

5.5 A Canonical Sequence

The results of this study are summarized in Fig. 5.15 which depicts the "canonical" evolution of a summertime ISO as well as the interaction of the ISO with 5–10-day westward propagating systems. Day 0 is defined arbitrarily as the day when ISO convection develops along the equator at 90°E. At this stage of the ISO evolution, the western Pacific Ocean is under suppressed convective conditions that can be attributed to the previous ISO cycle. The green arrows shown in the day 0 panel represent the low-level anomalous winds that characterize the Kelvin-Rossby wave packet that is associated with the ISO convection. Along the equator, the Kelvin component is manifest as anomalous easterlies and westerlies to the east and west of the equatorial convection. Off the equator, cyclonic Rossby cells are located in both hemispheres to the west of the equatorial convection while anti-cyclonic Rossby cells are found to the west of suppressed equatorial convection.

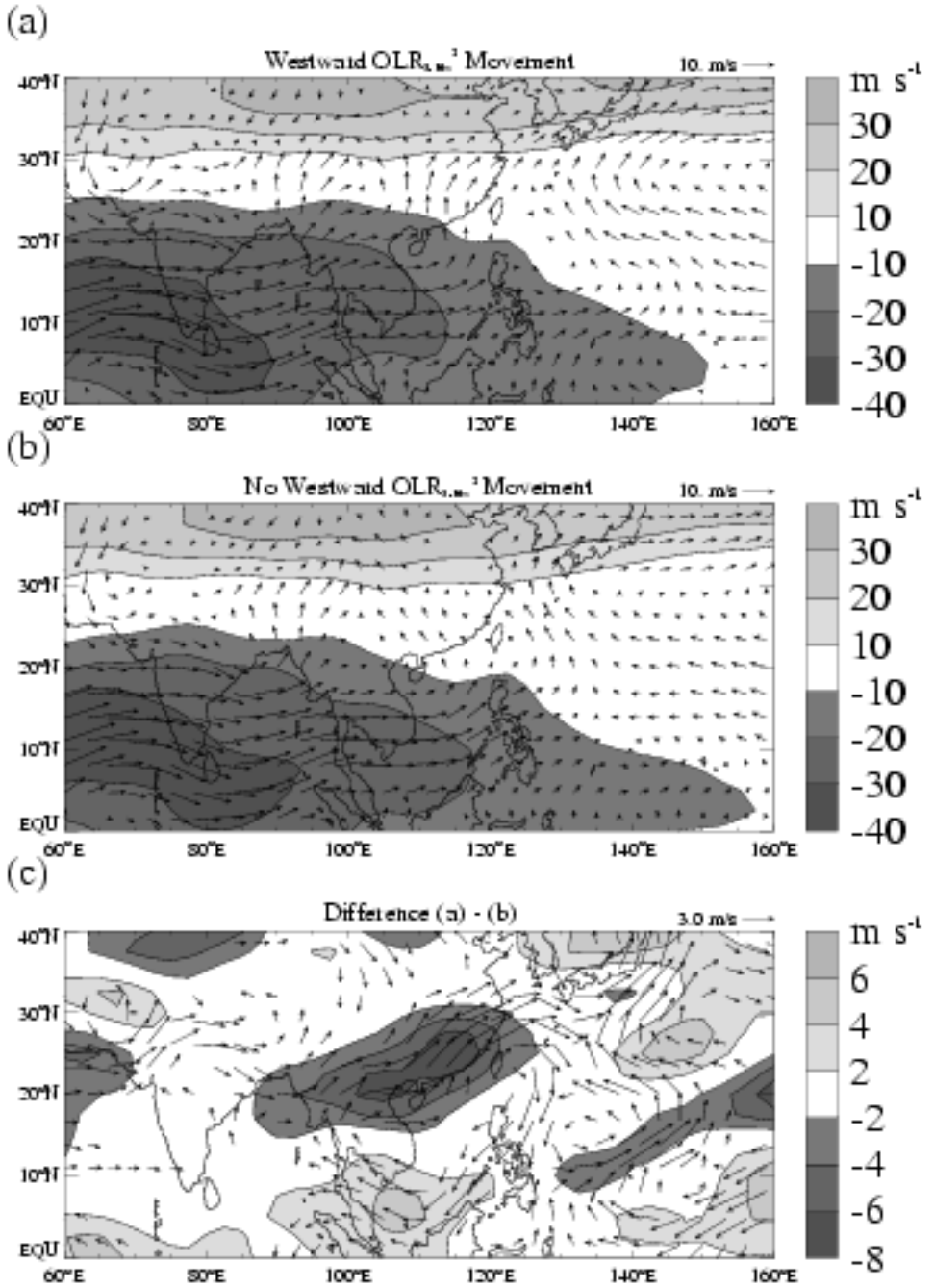

Figure 5.14. Zonal vertical wind shear and 850-mb wind composites based on average circulation for 20 days after statistically significant $OLR_{5-10w}{}^2$ peak at 120°–130°E, 10°–20°N. (a) Composite for times when $OLR_{5-10w}{}^2$ exhibits westward movement after peak in western Pacific Ocean; 17 events. (b) Composite for times when $OLR_{5-10w}{}^2$ does not exhibit westward movement; 26 events. (c) Difference map of (a) – (b).

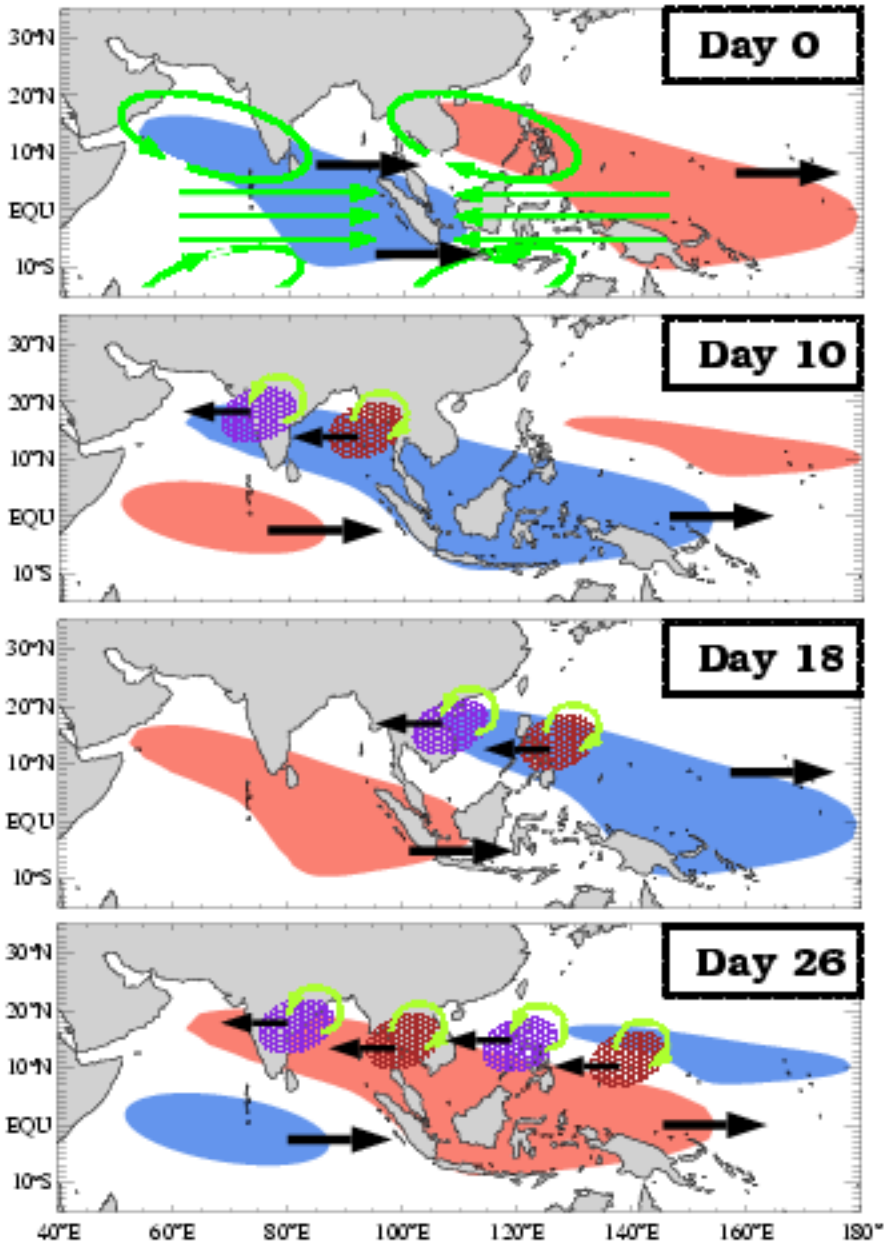

Figure 5.15. Canonical evolution of summertime ISO, including modulation of westward propagating synoptic-scale waves. Four panels shown at 0, 10, 18, 26 days following development of anomalous convection at 75°E along the equator, the abitrary beginning of ISO cycle. Light blue and light red indicate anomalous ISO convection and suppressed convection, respectively. Purple and brown represent synoptic-scale convection and suppressed convection. Black arrows show direction of propagation of ISO and synoptic-scale systems. Green arrows show anomalous low-level circulation associated with ISO and synoptic-scale systems. The ISO circulation is only shown in the first panel.

The frictional surface convergence into the cyclonic Rossby cells generates large-scale lifting, leading to off-equatorial convection. The green arrows representing the canonical anomalous low-level winds are omitted in the remaining three maps for clarity, although they basically move eastward in the same orientation, coupled to the equatorial convection.

At day 10, the equatorial ISO convection is centered near 130°E and the off-equatorial convection is aligned along a northwestward tilting axis stretching across the Indian subcontinent to 20°N. The time period during which the off-equatorial ISO convection is located over India is an active period with precipitation typically well above the normal monsoonal rainfall. At least a portion of the increase in rainfall during an active period can be attributed to an increase in synoptic-scale storm activity, shown as purple ovals in Fig. 5.15. These systems are excited by ISO convection in conjunction with instabilities inherent to the strong easterly vertical wind shear that is prevalent across the Indian monsoon region at this time of year. The systems typically develop in the Bay of Bengal and propagate across the Indian subcontinent, often generating substantial precipitation.

The day 18 map represents the time when the ISO convection has moved out of the Indian Ocean region and has been replaced by suppressed convection. The equatorial ISO convection is approaching the dateline and the end of its life-time while the off-equatorial convection is now located over the South China Sea. Synoptic-scale wave activity has dissipated over the northern Indian Ocean, but is beginning to be excited over the western Pacific Ocean. About half the time, synoptic-scale waves that develop in the western Pacific Ocean propagate west over southeast Asia, typically losing strength, only to regain it upon reaching the warm waters of the Bay of Bengal. By day 26, a large-scale break period is seen over